Use of a Peptide Derived from Foot-and-Mouth Disease Virus for the Noninvasive Imaging of Human Cancer: Generation and Evaluation of 4-[^{18}F]Fluorobenzoyl A20FMDV2 for *In vivo* Imaging of Integrin $\alpha_v\beta_6$ Expression with Positron Emission Tomography

Sven H. Hausner,[1] Danielle DiCara,[2] Jan Marik,[1] John F. Marshall,[2] and Julie L. Sutcliffe[1]

[1]Department of Biomedical Engineering, University of California Davis, Davis, California and [2]Centre for Tumour Biology, Barts and the London, Queen Mary's School of Medicine and Dentistry, London, United Kingdom

Abstract

Expression of the epithelial-specific integrin $\alpha_v\beta_6$ is low or undetectable in most adult tissues but may be increased during wound healing and inflammation and is up-regulated dramatically by many different carcinomas, making $\alpha_v\beta_6$ a promising target for the *in vivo* detection of cancer using noninvasive imaging. In addition, $\alpha_v\beta_6$ is recognized as promoting invasion and correlates with aggressive behavior of human cancers and thus agents that recognize $\alpha_v\beta_6$ specifically *in vivo* will be an essential tool for the future management of $\alpha_v\beta_6$-positive cancers. Recently, we identified the peptide NAVPNLRGDLQVLAQKVART (A20FMDV2), derived from foot-and-mouth disease virus, as a potent inhibitor of $\alpha_v\beta_6$. Using flow cytometry and ELISA, we show that this peptide is highly selective, inhibiting $\alpha_v\beta_6$-ligand binding with a IC_{50} of 3 nmol/L, an activity 1,000-fold more selective for $\alpha_v\beta_6$ than for other RGD-directed integrins ($\alpha_v\beta_3$, $\alpha_v\beta_5$, and $\alpha_5\beta_1$). A20FMDV2 was radiolabeled on solid-phase using 4-[^{18}F]fluorobenzoic acid, injected into mice bearing both $\alpha_v\beta_6$-negative and $\alpha_v\beta_6$-positive (DX3puro/DX3puroβ6 cell lines) xenografts and imaged using a small animal positron emission tomography (PET) scanner. Rapid uptake (<30 min) and selective retention (>5 h) of radioactivity in the $\alpha_v\beta_6$-positive versus the $\alpha_v\beta_6$-negative tumor, together with fast renal elimination of nonspecifically bound activity, resulted in specific imaging of the $\alpha_v\beta_6$-positive neoplasm. These data suggest that PET imaging of $\alpha_v\beta_6$-positive tumors is feasible and will provide an important new tool for early detection and improved management of many types of cancers. [Cancer Res 2007;67(16):7833–40]

Introduction

The use of positron emission tomography (PET) is increasing as a major tool for the noninvasive clinical management of cancer. PET, based on the detection of γ-rays created during the annihilation in tissue of positrons from radioisotopes, such as ^{11}C, ^{15}O, and ^{18}F, has no depth limitations and provides quantifiable, three-dimensional images with near millimeter resolution (1). The most widely used PET radiopharmaceutical to date is 2-[^{18}F]fluoro-2-deoxy-D-glucose ([^{18}F]FDG; ref. 2). [^{18}F]FDG is preferentially trapped inside cells that have increased metabolic activity. However, as the metabolic activity of different cancers varies widely, new tumor-specific imaging targets are required (3). The problem is that there are few molecules that are expressed significantly more by many different types of cancer than their corresponding normal tissues and thus could serve as a suitable target for PET. The integrin $\alpha_v\beta_6$ represents such a target (4). Here, we describe the development of a novel $\alpha_v\beta_6$-specific peptide that was used successfully for imaging human $\alpha_v\beta_6$-expressing cancers with PET.

Integrins are expressed on the surface of most cells in the body and generate signals that regulate cell behavior, including motility, migration, survival, and invasion (5). Integrins bind to their extracellular ligands partly through the recognition of short peptide motifs, the most common of which is Arg-Gly-Asp (RGD; ref. 6). With a prominent role in tumor-related angiogenesis and metastasis, the integrin $\alpha_v\beta_3$ (the vitronectin receptor), naturally expressed at low levels on epithelial and mature endothelial cells but up-regulated in certain carcinomas, has received considerable attention in recent years (for recent reviews, see refs. 7, 8). Small, cyclic peptide ligands based on the RGD motif have been developed (6) and used for *in vivo* imaging (for example, refs. 9–11). For this study, we have chosen a novel, highly tissue-specific target, the integrin $\alpha_v\beta_6$: this epithelial-specific integrin is usually not detectable on nonpathologic tissues but may be up-regulated during wound healing, inflammation, and development and, significantly, is up-regulated by many cancers, including pancreatic, breast, ovarian, colon, and over 90% of oral squamous cell carcinoma (OSCC; refs. 12, 13). Furthermore, expression of $\alpha_v\beta_6$ correlates with development of metastasis in gastric cancer (14), is linked with a dramatic reduction in survival from colon cancer (15), and is reported to promote both the survival and invasive potential of carcinoma cells (12, 16–18). Thus, although its biological effects alone suggest that $\alpha_v\beta_6$ should be a therapeutic target, its strong expression on cancers versus normal tissue also identifies $\alpha_v\beta_6$ as a promising candidate for noninvasive imaging.

One cancer whose management is likely to benefit from $\alpha_v\beta_6$-specific PET imaging is OSCC. Nearly 400,000 new cases occur globally each year (19) and there is, approximately, a 50% mortality rate after 5 years, a rate that has remained relatively unchanged for decades (20). Treatment often involves mutilating surgery and, in most cases, recurrence can be traced to incomplete excision of the primary or an undetected second primary. Thus, novel detection and diagnosis strategies are needed desperately. As over 90% of OSCCs express $\alpha_v\beta_6$ strongly (12), most patients

Note: Supplementary data for this article are available at Cancer Research Online (http://cancerres.aacrjournals.org/).

S.H. Hausner and D. DiCara contributed equally to this work.

J.F. Marshall and J.L. Sutcliffe jointly supervised this study.

Requests for reprints: Julie L. Sutcliffe, Department of Biomedical Engineering, Genomics and Biomedical Sciences Facility, University of California Davis, 451 East Health Sciences Drive, Davis, CA 95616. Phone: 530-754-7107; Fax: 530-754-5739; E-mail: jlsutcliffe@ucdavis.edu and John F. Marshall, Centre for Tumour Biology, Institute of Cancer, Barts and the London, Queen Mary's School of Medicine and Dentistry, Charterhouse Square, London EC1M 6BQ, United Kingdom. E-mail: john.marshall@cancer.org.uk.

doi:10.1158/0008-5472.CAN-07-1026

would be suitable candidates for noninvasive imaging that would enable (*a*) improved image-guided surgery (*b*) better detection of second primaries or occult metastases, and (*c*) noninvasive follow-up to assess for recurrence.

In this study, we have developed a radiolabeled peptide for PET imaging. The advantages of peptides as targeting agents include their rapid clearance from tissues allowing for the maximal target/background ratio to be achieved in the shortest time frame, their minimal immunogenicity, and that they can be synthesized relatively easily to high purity. Furthermore, reliable, standard synthetic procedures allow the rapid incorporation of several radioisotope-containing 'prosthetic' groups into peptides (21–27). In particular, radiofluorination procedures, chiefly with 4-[^{18}F]fluorobenzoic acid ([^{18}F]FBA), have been developed recently that permit convenient synthesis and automated radiolabeling of PET imaging probes (21, 24).

In this report, we describe a 20–amino acid peptide, NAVPNLRGDLQVLAQKVART (A20FMDV2), as a first-generation radiotracer for targeting $\alpha_v\beta_6$ *in vivo*. The sequence, derived from the GH loop of an envelope protein of the foot-and-mouth disease virus (FMDV; serotype O isolate O_1BFS 1860; ref. 28), mediates FMDV infection by binding to $\alpha_v\beta_6$ (29–31). The key region of the loop, which is conserved in many FMDV serotypes (28, 32–35), is the RGDLXXL motif, where X indicates the location of a nonspecific amino acid. The highly conserved RGD triplet is recognized by eight different integrins, most notably by the widely expressed $\alpha_v\beta_3$ (6, 36). Phage display analysis identified the DLXXL sequence as a key moiety responsible for $\alpha_v\beta_6$ specificity while having only minimal interactions with $\alpha_v\beta_3$, $\alpha_v\beta_5$, and $\alpha_{IIb}\beta_3$ (33). Later studies confirmed the importance of the DLXXL region in $\alpha_v\beta_6$-dependent infection by FMDV (31).

The aim of this study was to show the feasibility of selective *in vivo* imaging of integrin $\alpha_v\beta_6$. For this purpose, the small linear peptide A20FMDV2 was synthesized and NH_2-terminally radiolabeled with [^{18}F]FBA on solid-phase to yield [^{18}F]FBA-A20FMDV2. Specificity of A20FMDV2 (and [^{19}F]FBA-A20FMDV2) for integrin $\alpha_v\beta_6$ was determined by ELISA and inhibition of cell binding assays. The potential of [^{18}F]FBA-A20FMDV2 for use as an imaging agent was shown in mice bearing matched $\alpha_v\beta_6$-positive and $\alpha_v\beta_6$-negative human xenografts. In addition, biodistribution studies were done and the *in vivo* stability of [^{18}F]FBA-A20FMDV2 was evaluated. These data identify [^{18}F]FBA-A20FMDV2 as a promising agent for noninvasive imaging of $\alpha_v\beta_6$ *in vivo*.

Materials and Methods

Reagents and cell lines. The human melanoma cell line DX3 was infected with pBabe retroviruses encoding puromycin resistance or, in addition, cDNA for human β6 as described previously (16). Cells were selected in puromycin (1.25 μg/mL) followed by magnetic bead sorting, using 10D5 (mouse anti-$\alpha_v\beta_6$; Chemicon International), according to the manufacturer's instructions (Dynal; Invitrogen). Recombinant soluble $\alpha_v\beta_6$ (rs$\alpha_v\beta_6$) was generated from CHOβ6 cells (a kind gift from Dr. Dean Sheppard, University of California San Francisco, San Francisco, CA) as described previously (37). Recombinant soluble $\alpha_v\beta_3$, $\alpha_v\beta_5$, and $\alpha_5\beta_1$ were a kind gift from Genentech. Mouse monoclonal anti-αv antibody (clone P2W7) was generated in the JFM laboratory. Monoclonal antibodies to the integrins $\alpha_v\beta_3$ (LM609), $\alpha_v\beta_5$ (P1F6), $\alpha_v\beta_6$ (10D5), and $\alpha_5\beta_1$ (JBS5 and P1D6) were purchased from Chemicon International. Mouse anti-$\alpha_v\beta_8$ (14E5) was a kind gift from Dr. Steve Nishimura (University of California San Francisco). IgG1-κ (clone MOPC 21) and ExtrAvidin-peroxidase conjugate were purchased from Sigma-Aldrich. Alexa Fluor 488–conjugated goat anti-mouse IgG was obtained from Molecular Probes (Invitrogen). MaxiSorp 96-well microtiter plates were used for ELISA (Nunc). 3,3′5,5′-Tetramethylbenzidine (TMB) substrate was purchased from DakoCytomation. Reagents for peptide synthesis were obtained from NovaBiochem, Sigma-Aldrich, and GL China. Jupiter Proteo reverse-phase columns (90 Å, 250 × 4.6 mm × 4 μm and 250 × 10 mm × 10 μm; Phenomenex) were used for reverse-phase HPLC (RP-HPLC) purification. Radio-HPLC was monitored with a Flow-Count Radio HPLC Detector (Bioscan). Mass spectra were obtained on a Bruker Biflex 3. [^{18}F]FDG was purchased from PETNet. PET scans were done on a microPET Focus120 scanner (Siemens Medical Solutions USA) and data were processed with the accompanying ASIpro software. Biodistribution samples were analyzed on a Wizard 1470 Automatic Gamma Counter (Perkin-Elmer). Flow cytometry was done on a FACScan (Becton Dickinson) or a FACSCalibur (Becton Dickinson) and analyzed with CellQuest software.

Peptide synthesis. Manual synthesis of A20FMDV2 followed standard Fmoc solid-phase peptide synthesis chemistries using Rink amide PEG-PS resin yielding the C-terminal amide. N-terminal labeling with 4-[^{19}F] fluorobenzoic acid or D-biotin (separated by an ε-amino-hexanoic acid spacer) followed the same procedures. Side chain protections of the amino acids used were the following: asparagine, glutamine: trityl; arginine: 2,2,4,6,7-pentamethyldihydrobenzofuran-5-sulfonyl; aspartic acid: *tert*-butyl; lysine: *tert*-butoxycarbonyl; and threonine: *tert*-butyl. Either HOBt/DIC or HBTU/DIPEA were used as coupling reagents. Coupling was monitored by picrylsulfonic acid test (38). Removal of the Fmoc protecting group was achieved with piperidine (20% v/v in dimethylformamide). Removal of the side chain protecting groups and cleavage off the resin was achieved with trifluoroacetic acid (TFA)/ethanedithiol/water/triisopropylsilane 94:2.5:2.5:1 (v/v/v/v). Purification on analytic and semipreparative scale was carried out by gradient RP-HPLC. Products were eluted with a linear gradient starting at 10% solvent B (for 2 min), increasing to 90% over 30 min. Solvent A: 0.05% TFA in water (v/v); solvent B: 0.005% TFA in water/acetonitrile 1:9 (v/v/v). Nonradiolabeled compounds were characterized by electrospray ionization or matrix-assisted laser desorption/ionization (MALDI) mass spectrometry. Cyclo-(RGDy(Me)K) was synthesized as described previously (39).

Competitive binding ELISA. The potencies of the parent peptide A20FMDV2 and [^{19}F]FBA-A20FMDV2 were compared by competitive binding ELISA. The peptides were allowed to compete during 1 h for binding to integrins $\alpha_v\beta_6$, $\alpha_v\beta_3$, $\alpha_v\beta_5$, and $\alpha_5\beta_1$ with biotinylated natural ligands, either fibronectin ($\alpha_v\beta_6$ and $\alpha_5\beta_1$) or vitronectin ($\alpha_v\beta_3$ and $\alpha_v\beta_5$). Briefly, a 96-well plate was coated with 50 μL/well of 5 μg/mL P2W7 antibody (for α_v integrins) or JBS5 (for $\alpha_5\beta_1$) in PBS at 37°C for 1 h. The plate was washed three times with PBS followed by treatment with PBS containing 5% bovine serum albumin (BSA; fraction V; w/v) and 1% Tween 20 (v/v) at room temperature for 3 h to block nonspecific binding. The plate was washed as above and coated with 50 μL/well integrin in wash buffer (WaB) and then washed three times with WaB. WaB consisted of a solution of 2 mmol/L Tris buffer (pH 7.6), 150 mmol/L sodium chloride, 1 mmol/L manganese chloride, and 0.1% Tween 20 (v/v) in deionized water. For the competition experiment, triplicate wells were coated with 50 μL/well of a mixture of equal volumes of biotinylated fibronectin (BtFn) or vitronectin (BtVn) in conjugate buffer, consisting of 1% BSA (fraction V; w/v) in WaB, and a serial dilution of peptide stock [2 mmol/L; 10% DMSO (v/v) in PBS or water]. Wells containing no peptide, no peptide and no antibody, or no peptide and no ligand served as controls. The plate was incubated for 1 h at room temperature and washed three times with WaB before ExtrAvidin-horseradish peroxidase conjugate was added (50 μL/well, 1:1,000 dilution in conjugate buffer) at room temperature for 1 h. After washing with WaB as above, bound BtFn (or BtVn) was detected by addition of TMB (50 μL/well) and incubation for 10 to 15 min. The reaction was terminated by adding 50 μL/well 1N sulfuric acid and absorbance was measured at 450 nm (yellow color of acidified oxidized TMB). Experiments were carried out a minimum of two times. Calculations of IC_{50} values are based on data analysis with Prism software (GraphPad Software).

Cell binding assays. Various concentrations of biotinylated A20FMDV2 (Bt-A20FMDV2) were added to 2×10^5 DX3puro and DX3puroβ6 cells for 30 min in DMEM supplemented with 0.1% NaN_3 (w/v) and 0.1% BSA (w/v) before washing three times in same. Bound peptide was detected with

mouse anti-biotin antibody (1:100 dilution, 30 min at 4°C; Jackson ImmunoResearch). After washing off unbound antibody, Alexa Fluor 488–conjugated antimouse IgG was added for 30 min before washing three times and analyzing by flow cytometry.

Flow cytometry analysis. Integrin expression was determined by flow cytometry as described previously (16). Briefly, primary antibodies (10 μg/mL, 4°C) were added for 30 min, and the cells were washed and incubated with fluorescently labeled secondary antibody for an additional 30 min. Cells were washed, resuspended, and analyzed by flow cytometry.

Radiochemistry. N-terminal solid-phase [^{18}F]fluorobenzoyl radiolabeling of A20FMDV2 was adapted from a previously published method (21). Briefly, the no-carrier-added (n.c.a.) [^{18}F]FBA was synthesized from ethyl 4-(trimethylammoniumtrifluoromethanesulfonate) benzoate followed by saponification of the ethyl ester protecting group. The synthesis was done on a 300 to 700 mCi scale using a chemistry process control unit (CPCU; Siemens Medical Solutions USA). The [^{18}F]FBA was redissolved in dimethylformamide and coupled to the peptide attached to the solid support (1.5–2.0 mg resin) using HATU/DIPEA. The resin, enclosed in a 1 mL fritted syringe, was shaken continuously for 25 min at room temperature and washed thoroughly with dimethylformamide and methanol. The product was cleaved from the solid support using TFA/triisopropylsilane/water 95:2.5:2.5 (v/v/v) for 30 min at 30° to 40°C. The cleavage mixture was evaporated using a stream of nitrogen and the crude product was purified on semipreparative RP-HPLC [27% acetonitrile/0.05% TFA in water (v/v/v)].

***In vivo* studies.** Male athymic nude mice (*nu/nu*; Charles River Laboratories) were inoculated s.c. on opposite flanks in the shoulder region with 3×10^6 DX3puro or DX3puroβ6 cells in 100 μL serum-free DMEM (Mediatech). Cell lines were analyzed by flow cytometry before injection to confirm integrin expression patterns. Food and water were available *ad libitum*. Imaging was conducted between 2 and 5 weeks after injection on mice weighing 25 to 35 g, once tumors had reached a minimum diameter of 5 mm. Animal care and treatment followed protocols approved by the Animal Care and Use Committee of the University of California Davis (Davis, CA).

Urine and blood analysis. Urine was collected at various points. Aliquots (20 μL) were analyzed by RP-HPLC as described in the peptide synthesis section. For *in vivo* serum stability studies, blood was collected at various points and mixed with an equal volume of acetonitrile, and solids were removed by centrifugation followed by RP-HPLC analysis of the supernatant.

Biodistribution studies. Nine mice were anesthetized with 3% isoflurane and inoculated i.v. via the tail vein through a catheter prepared from a 30-gauge needle and PE 10 tubing (Becton Dickinson) with 15 to 30 μCi [^{18}F]FBA-A20FMDV2 diluted in 150 to 200 μL saline. At 1, 2, and 4 h after injection, mice were killed, tumors and other tissues were excised, and the associated radioactivity was measured in a gamma counter calibrated against aliquots of known activity (n = 3 mice per time point). Results, based on decay-corrected counts and tissue weights, are expressed as percent of injected dose detected per gram of tissue (% ID/g). Two-tailed Student's t tests were done to evaluate tumor uptake ratios for statistical significance.

MicroPET imaging studies. Mice (n = 6) were anesthetized with 3% isoflurane and maintained at 1.5% to 2.0%. [^{18}F]FBA-A20FMDV2 or [^{18}F]FDG (100–250 μCi) in 100 to 200 μL saline or PBS was injected i.v. For blocking studies, [^{19}F]FBA-A20FMDV2 (10 mg/mL in saline, 90 μL) was injected by catheter in one animal 10 min before the radiotracer. The animals were placed in a head-first, prone position on the scanner bed. Body temperature was measured by a rectal probe and maintained with a heating pad, supplemented by a heating lamp. Dynamic 15-min scans were acquired at various time points, from immediately after injection up to 6.5 h.

List mode scanner data were binned into sinograms using Fourier Rebinning (40) and then reconstructed into a three-dimensional volumetric image using an iterative Maximum a-Posteriori algorithm (18 iterations after 4 iterations of three-dimensional ordered subset expectation maximization; ref. 41). Pixel size was set to 0.8 mm, and smoothing parameter (β) was set to 0.1. Calibration to activity concentration was achieved using cylindrical phantoms with volumes similar to mice (30 mL).

Results

Competitive binding ELISA. In a recent study, we reported that the N terminus of A20FMDV2 is not involved significantly in binding to $\alpha_v\beta_6$ (4). To confirm whether the addition of the prosthetic 4-fluorobenzoyl group (FBA) to the N terminus of A20FMDV2 affected peptide specificity or efficacy, modified ([^{19}F]FBA-A20FMDV2) and unmodified (A20FMDV2) peptides were tested for their ability to inhibit binding of biotinylated fibronectin to immobilized rs$\alpha_v\beta_6$. In addition, the ability of peptides to inhibit biotinylated ligands binding to immobilized recombinant $\alpha_v\beta_3$, $\alpha_v\beta_5$, and $\alpha_5\beta_1$ was also tested. The α_v-binding peptide cyclo-(RGDy(Me)K) was included as a control (36, 39). Figure 1 shows that addition of [^{19}F]FBA to A20FMDV2 did not affect potency; thus, both A20FMDV2 and [^{19}F]FBA-A20FMDV2 inhibited binding of biotinylated fibronectin to rs$\alpha_v\beta_6$ with a IC_{50} of 3 ± 1 nmol/L. In contrast, the ability of A20FMDV2 and [^{19}F]FBA-A20FMDV2 to inhibit the other integrins required >1,000-fold higher concentrations of peptide (IC_{50} of $\alpha_v\beta_3$, $\alpha_v\beta_5$, and $\alpha_5\beta_1$, >10 μmol/L). By comparison, the cyclo-(RGDy(Me)K) control peptide exhibited comparably strong inhibition of all three α_v integrins with limited selectivity. No significant inhibition of $\alpha_5\beta_1$ was observed for any peptide tested.

Characterization and use of DX3puro and DX3puroβ6 cell lines. Having established that A20FMDV2 was highly selective for recombinant $\alpha_v\beta_6$, it was necessary to confirm that A20FMDV2 was also specific for $\alpha_v\beta_6$ expressed at the cell surface. We therefore generated a highly stringent cell-based selection method that could be used both *in vitro* and *in vivo* for the analysis of potential $\alpha_v\beta_6$-targeting agents. The human melanoma cell line DX3 (42) was transduced retrovirally with cDNA encoding the puromycin resistance gene or, in addition, cDNA encoding the human β_6 integrin subunit to create DX3puro and DX3puroβ6 cell lines, respectively. These cells were analyzed by flow cytometry for expression of the RGD-directed integrins $\alpha_v\beta_3$, $\alpha_v\beta_5$, $\alpha_v\beta_6$, $\alpha_v\beta_8$, and $\alpha_5\beta_1$. Figure 2*A* shows that there was equal expression of each of these integrins on both cell lines except for $\alpha_v\beta_6$, which was expressed only by DX3puroβ6 cells. Figure 2*B* shows that Bt-A20FMDV2 bound well to DX3puroβ6 even at a low concentration of 1 nmol/L, whereas even at 100 nmol/L, no binding to DX3puro was observed. Because DX3puro expresses similar levels of $\alpha_v\beta_3$, $\alpha_v\beta_5$, $\alpha_v\beta_8$, and $\alpha_5\beta_1$ as DX3puroβ6, these data suggest that A20FMDV2 is highly selective for $\alpha_v\beta_6$.

Radiosynthesis of [^{18}F]FBA-A20FMDV2. Fully automated synthesis of [^{18}F]FBA was achieved in a synthesis time of 50 min with a 70% decay-corrected radiochemical yield and >99% radiochemical purity. Solid-phase coupling to H_2N-A20FMDV2 yielded [^{18}F]FBA-A20FMDV2 in a decay-corrected radiochemical yield of 3.6% and radiochemical purity >98% after RP-HPLC purification (n = 13, specific activity 37 GBq/μmol; Supplementary Fig. S1). Total synthesis and purification time was 130 min since end of bombardment.

***In vivo* studies: urine and blood analysis and biodistribution.** Athymic mice bearing paired DX3puro and DX3puroβ6 xenografts were injected with [^{18}F]FBA-A20FMDV2, major organs were dissected, and radioactivity was measured. Urine samples were collected during biodistribution and imaging studies at various time points between 1 to 3 h after injection and analyzed by HPLC. Samples collected 1 h after injection contained, on average, 45 ± 23% of the administered activity (decay corrected). Levels increased to 63 ± 8% after 3 h. In some cases, over two thirds of the radioactivity was observed in

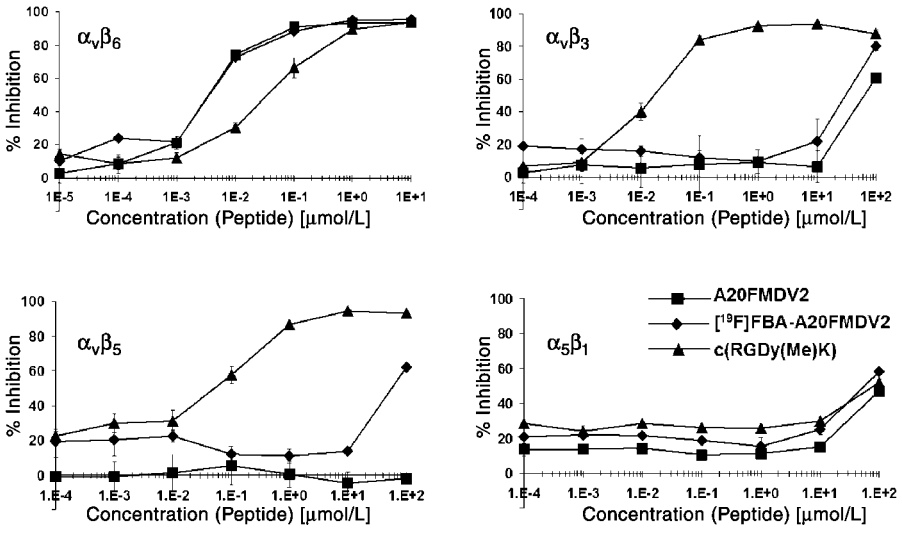

Peptide	$\alpha_v\beta_6$	$\alpha_v\beta_3$	$\alpha_v\beta_5$	$\alpha_5\beta_1$
A20FMDV2	3 ± 1 nmol/L	>10 μmol/L	>100 μmol/L	>10 μmol/L
[^{19}F]FBA-A20FMDV2	3 ± 1 nmol/L	>10 μmol/L	>10 μmol/L	>10 μmol/L
cyclo-(RGDy(Me)K)	35 ± 15 nmol/L	16 ± 5 nmol/L	90 ± 30 nmol/L	>10 μmol/L

Figure 1. Comparison of the ability of A20FMDV2, [^{19}F]FBA-A20FMDV2, and cyclo-(RGDy(Me)K) peptides to inhibit binding of biotinylated ligands to immobilized $\alpha_v\beta_6$, $\alpha_v\beta_3$, $\alpha_v\beta_5$, and $\alpha_5\beta_1$ integrins. The $\alpha_v\beta_6$ assay was conducted in the range of 10 pmol/L to 10 μmol/L, all others in the range of 100 pmol/L to 100 μmol/L. *Points,* % inhibition; *bars,* SD (smaller than the size of the symbol for some data points). IC_{50} values for inhibiting the ability of specific integrins to bind to biotinylated ligands are presented.

the urine as early as 1 h after injection. The radioactivity was distributed approximately equally between three metabolites with retention times of 9.0, 10.4, and 10.8 min, respectively, as indicated by RP-HPLC (Supplementary Fig. S1). None of the urine samples analyzed contained any unmetabolized [^{18}F]FBA-A20FMDV2 (R_t = 16.6 min).

Blood samples revealed rapid clearance of radioactivity from the bloodstream; over 95% of the injected dose had been cleared within 10 min after injection (data not shown). Biodistribution data confirmed rapid elimination from the blood and renal excretion as the major route of clearance as is evident from the high % ID/g detected in the urine (1,082%, 331%, and 74.1% ID/g at 1, 2, and 4 h, respectively; Table 1). By 1 h after injection, most of the activity already had passed through the kidneys (3.56% ID/g) and no significant renal retention was observed; at 2 and 4 h, the levels had dropped to 0.55% and 0.15% ID/g, respectively. Uptake in the $\alpha_v\beta_6$-expressing tumor was 0.66% ID/g at 1 h, dropping to 0.28% and 0.06% ID/g at 2 and 4 h, respectively. Significantly, uptake in the control tumor stayed at less than one third of the $\alpha_v\beta_6$-expressing tumor at all time points (0.21%, 0.07%, and 0.02% ID/g at 1, 2, and 4 h, respectively), remaining near or below the levels detected for the blood (0.27%, 0.06%, and 0.03% ID/g at 1, 2, and 4 h, respectively), as shown in Fig. 3. High levels of activity were detected in the gall bladder (1 h, 15.1% ID/g; 4 h, 1.97% ID/g), whereas liver, spleen, and bone showed no significant levels of radioactivity.

MicroPET scans. Representative, decay-corrected transaxial images for n.c.a. [^{18}F]FBA-A20FMDV2 are shown in Fig. 4. Nonspecific activity cleared quickly from blood resulting in a low background. Images with good positive tumor/negative tumor and positive tumor/background ratios generally were obtained 30 to 90 min after injection (Fig. 4*A*). As exemplified in Fig. 4*B*, uptake of activity in the tumor tissue was fast, usually <20 min. Activity was retained in the $\alpha_v\beta_6$-expressing tumor over extended periods. Images with a clearly identifiable $\alpha_v\beta_6$-positive tumor routinely were obtained as early as 15 min and as late as 5 h after injection. Based on volume-of-interest analysis, the ratio of accumulated activity in the $\alpha_v\beta_6$-expressing tumor versus background improved steadily over time (1 h, 2.2:1; 3 h, 3.5:1). These observations paralleled the results seen in the biodistribution; thus, organs showing major activity by microPET were kidneys, bladder (urine), and gall bladder (data not shown).

To confirm that differences seen between the tumors with [^{18}F]FBA-A20FMDV2 were not caused by differences in tumor viability, several of the mice also were imaged with the metabolic tracer [^{18}F]FDG. MicroPET scans 1 h after injection showed no differences in [^{18}F]FDG uptake between the positive and the negative tumor, suggesting similar blood supplies and metabolic rates in both (Fig. 4*A, 3* and *4*); uptake ratios were 1.0:1 ($\alpha_v\beta_6$-expressing tumor/control tumor) and 1.8:1 ($\alpha_v\beta_6$-expressing tumor/background).

When [^{19}F]FBA-A20FMDV2 was injected i.v. at 30 mg/kg 10 min before [^{18}F]FBA-A20FMDV2, a 32% reduction in uptake of radiotracer by the $\alpha_v\beta_6$-expressing tumor was observed. In contrast, uptake in the control tumor remained unchanged (−1%; data not shown).

Discussion

The integrin $\alpha_v\beta_6$ promotes invasion *in vitro* and *in vivo* (12, 17) and is associated with development of metastases from gastric cancer (14) and poor survival from colon cancer (15). Moreover, $\alpha_v\beta_6$ is up-regulated significantly on many carcinomas, including >90% of oral cancers, in contrast to the corresponding normal tissue that has little or no expression (12). These data identify $\alpha_v\beta_6$ as a major new target for noninvasive imaging of many types of cancers and highlight that the ability to accurately and rapidly identify $\alpha_v\beta_6$-positive neoplasms will be an essential component of the management of many types of carcinoma. Here, we describe the first *in vivo* imaging studies of human $\alpha_v\beta_6$-expressing cancers.

Use of radiolabeled peptides as molecular imaging agents holds great promise as they combine low immunogenicity with efficient transport to the tumor and good clearance characteristics. In fact, previous studies successfully imaged $\alpha_v\beta_3$ on human xenografts using ^{18}F-labeled peptides (9, 10). Recently, we examined the structure and function of 20-mer peptides that were designed around the RGD motif of high-affinity ligands for $\alpha_v\beta_6$ (4). We determined that A20FMDV2, derived from the GH loop of FMDV (29–31), had a high affinity for binding to $\alpha_v\beta_6$ and a high capacity for inhibiting $\alpha_v\beta_6$-dependent adhesion. We also reported that the interface of the peptide with $\alpha_v\beta_6$ required the RGD motif and that the adjacent DLXXL/I motif (33–35) needs to be part of a C-terminal helix; residues N-terminal to the RGD motif were not implicated in binding. We considered therefore that A20FMDV2 might be a useful agent for the imaging of $\alpha_v\beta_6$-positive tumors and, further, that attachment of a prosthetic group at the N-terminus, readily accessible for chemical modifications (21), should cause little interference with peptide function. *In vitro* comparison of [^{19}F]FBA-A20FMDV2 with A20FMDV2 in competitive ELISA confirmed that the addition of the FBA prosthetic group to the N-terminus had no deleterious effect on potency, with the IC_{50} for inhibiting $\alpha_v\beta_6$ function remaining at 3 ± 1 nmol/L. Especially encouraging was the >1,000-fold specificity for $\alpha_v\beta_6$ of [^{19}F]FBA-A20FMDV2 and A20FMDV2 versus other RGD-directed integrins tested, compared with cyclo-(RGDy(Me)K), which exhibited relatively poor selectivity (Fig. 1).

The focus of this study was noninvasive *in vivo* microPET imaging of $\alpha_v\beta_6$. Thus, it was necessary to determine that A20FMDV2 bound specifically to cellular $\alpha_v\beta_6$. Because $\alpha_v\beta_6$ is one of eight RGD-directed integrins, we developed a highly stringent selection method to ensure specificity for $\alpha_v\beta_6$. We generated the DX3puro/DX3puroβ6 pair of cell lines, which both express similar levels of four RGD-directed integrins ($\alpha_v\beta_3$, $\alpha_v\beta_5$, $\alpha_v\beta_8$, and $\alpha_5\beta_1$), whereas DX3puroβ6 also expresses $\alpha_v\beta_6$ (Fig. 2*A*). Using these cell lines, N-terminally biotinylated-A20FMDV2 exhibited strong binding to DX3puroβ6, even at 1 nmol/L, but no binding to the $\alpha_v\beta_6$-negative control line even at 100-fold concentrations (Fig. 2*B*). Thus, A20FMDV2 binding is highly specific for cellular $\alpha_v\beta_6$.

Using mice bearing both DX3puro and DX3puroβ6 tumors on opposite shoulders allowed direct comparison between the $\alpha_v\beta_6$-expressing tumor and a negative control in the same animal. Importantly, xenografts of DX3puroβ6 maintain high expression of $\alpha_v\beta_6$ (data not shown). Using [^{18}F]FBA-A20FMDV2, we were able to successfully and selectively image the $\alpha_v\beta_6$-expressing tumor. Uptake in the target tissue occurred rapidly, together with efficient washout of nonspecific activity from the surrounding tissue. Within <30 min, the $\alpha_v\beta_6$-positive xenograft was clearly visible and, more importantly, showed a stronger signal than the $\alpha_v\beta_6$-negative

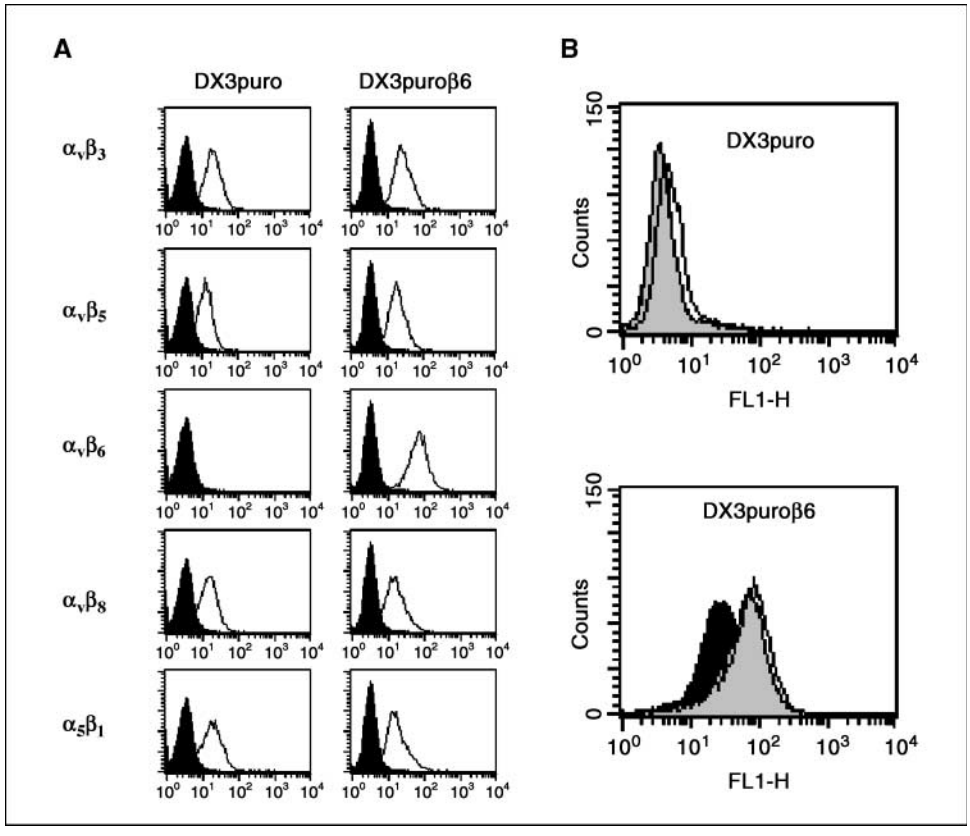

Figure 2. Characterization and use of DX3puro and DX3puroβ6 cell lines. *A,* integrin expression (*white histogram*) by DX3puro and DX3puroβ6 cells was determined by flow cytometry using antibodies to $\alpha_v\beta_3$ (LM609), $\alpha_v\beta_5$ (P1F6), $\alpha_v\beta_6$ (10D5), $\alpha_v\beta_8$ (14E5), and $\alpha_5\beta_1$ (P1D6). Mouse IgG (*black histogram*) was used as antibody control. Data show that both cell lines express similar levels of all integrins tested except $\alpha_v\beta_6$, which is expressed only by DX3puroβ6 cells. *B,* N-terminally biotinylated-A20FMDV2 peptide was added to DX3puro or DX3puroβ6 cells at 1 nmol/L (*black histogram*), 10 nmol/L (*gray histogram*), 100 nmol/L (*white histogram*) concentrations. Bound peptide was detected as described and cells were analyzed by flow cytometry. Note that A20FMDV2 is specific for DX3puroβ6 cells at all concentrations used.

Table 1. Biodistribution data for [^{18}F]FBA-A20FMDV2 after i.v. injection into male *nu/nu* mice (n = 3 per time point) bearing pairs of DX3puroβ6 ($\alpha_v\beta_6$) and DX3puro (control) xenografts

Tissue	% ID/g ± SD		
	1 h After injection	2 h After injection	4 h After injection
Tumor ($\alpha_v\beta_6$)	0.66 ± 0.09*	0.28 ± 0.03†	0.06 ± 0.00‡
Tumor (control)	0.21 ± 0.07*	0.07 ± 0.02†	0.02 ± 0.01‡
Blood	0.27 ± 0.08	0.06 ± 0.03	0.03 ± 0.02
Liver	0.63 ± 0.18	0.12 ± 0.02	0.03 ± 0.01
Kidney	3.56 ± 1.38	0.55 ± 0.16	0.15 ± 0.09
Pancreas	0.23 ± 0.12	0.13 ± 0.12	0.02 ± 0.01
Heart	0.31 ± 0.13	0.07 ± 0.03	0.02 ± 0.01
Spleen	0.07 ± 0.02	0.05 ± 0.03	0.01 ± 0.00
Brain	0.02 ± 0.02	0.01 ± 0.01	0.00 ± 0.00
Stomach	1.33 ± 0.22	0.42 ± 0.08	0.22 ± 0.13
Bone	0.29 ± 0.11	0.18 ± 0.14	0.03 ± 0.02
Muscle	0.56 ± 0.21	0.22 ± 0.14	0.08 ± 0.03
Gall bladder	15.05 ± 17.29	8.67 ± 4.10	1.97 ± 3.17
Urine	1,081.91 ± 278.51	331.39 ± 143.10	74.07 ± 70.53
Bladder	8.25 ± 5.44	7.27 ± 4.92	5.14 ± 6.73

*P = 0.0023.
†P = 0.0003.
‡P = 0.0002.

control tumor throughout the study. The images in Fig. 4 and the biodistribution data depicted in Fig. 3 show a clear preference of the probe for the $\alpha_v\beta_6$-expressing tumor in this stringent *in vivo* model. Such data suggest a high affinity of the tracer for the target receptor. We confirmed that differences in tracer uptake are not due to differences in vasculature or metabolism as [^{18}F]FDG signals were similar for $\alpha_v\beta_6$-positive and $\alpha_v\beta_6$-negative tumors (Fig. 4*A*).

A signal ($\alpha_v\beta_6$-expressing tumor) to background ratio of 1.8:1 was achieved with [^{18}F]FBA-A20FMDV2 within 10 min (data not shown); however, biodistribution and radio-HPLC analysis of urine samples confirmed the rapid renal clearance as seen in the microPET imaging. Rapid excretion of nonspecifically bound radioactivity is a desirable characteristic of a radiotracer because it reduces the radiation exposure of the subject and improves the signal-to-noise ratio of PET images. This can be seen for [^{18}F]FBA-A20FMDV2 by comparing the images obtained at 50 min and 3 h (Fig. 4*B*). However, the [^{18}F]FBA-A20FMDV2 was broken down rapidly into three radioactive metabolites and excreted in the urine. No unmetabolized [^{18}F]FBA-A20FMDV2 and no free [^{18}F]FBA were detected in any urine sample (Supplementary Fig. S1). Although we did not confirm the sequences of the metabolites in urine, a similar cleavage pattern was observed in *ex vivo* cleavage tests of [^{19}F]FBA-A20FMDV2 with chymotrypsin (data not shown). Predictive software (43) suggests that a likely cleavage site would be between the leucine and glutamine of DLQVL, thus destroying the site in the peptide implicated in $\alpha_v\beta_6$ specificity (33) and affinity of binding (4). The resultant N-terminal peptide ([^{18}F]FBA-NAVPNLRGDL) might have activity against other RGD-directed integrins. The lack of retention of radioactivity in the control versus the $\alpha_v\beta_6$-positive tumor suggests that this possible scenario is not of significance in our studies.

By injecting [^{19}F]FBA-A20FMDV2 before the radiotracer, we were able to reduce uptake of radioactivity in the $\alpha_v\beta_6$-expressing tumor by 32%, whereas uptake in the control tumor remained unchanged (data not shown). Because the *in vitro* studies showed [^{19}F]FBA-A20FMDV2 exhibiting a >1,000-fold higher affinity for $\alpha_v\beta_6$ over $\alpha_v\beta_3$, $\alpha_v\beta_5$, and $\alpha_5\beta_1$, these data support strongly that the positron-emitting [^{18}F]FBA-A20FMDV2 is binding $\alpha_v\beta_6$ selectively *in vivo*. Although [^{19}F]FBA-A20FMDV2 caused a significant reduction in uptake of [^{18}F]FBA-A20FMDV2, full blockage was not observed probably due to the rapid metabolism as noted in the urine and blood analysis.

The rapid removal from serum of unbound and nonspecifically bound activity contributed significantly to the rapid generation of a $\alpha_v\beta_6$-expressing tumor/background ratio of 2.2:1 (Fig. 4*B*). However, the high rate of degradation and clearance of the [^{18}F]FBA-A20FMDV2 reduced the amount of intact imaging probe available in the circulation that can reach the target tissue, suggesting that variants of A20FMDV2 with improved pharmacokinetics may achieve even better results. Thus, as a first-generation radiotracer, [^{18}F]FBA-A20FMDV2 exhibited several desirable characteristics: rapid uptake and persistence of radioactivity selectively in the $\alpha_v\beta_6$-expressing tumor together with good washout from the surrounding tissue and fast, predominantly renal clearance of nonspecifically bound activity. Moreover, selectivity for the $\alpha_v\beta_6$-expressing tumor was combined with tumor/background ratios comparable with, or even slightly better than, that observed for [^{18}F]FDG (2.2:1 versus 1.8:1). Although [^{18}F]FBA-A20FMDV2 was successful, we anticipate that modifications of this peptide, to improve the biological stability while maintaining $\alpha_v\beta_6$-specificity, will result in improved targeted imaging agents.

Conclusion

Accumulating data show that $\alpha_v\beta_6$ promotes the invasive phenotype of epithelial cancer cells. As the expression of the proinvasive integrin $\alpha_v\beta_6$ is significantly up-regulated by many

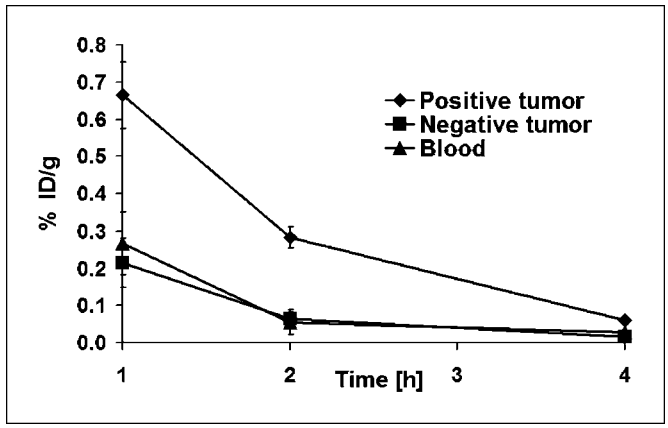

Figure 3. Comparison of the biodistribution of [^{18}F]FBA-A20FMDV2 in $\alpha_v\beta_6$-expressing (positive) tumor, negative control tumor, and blood in male *nu/nu* nude mice. *Points,* % ID/g; *bars,* SD (smaller than the size of the symbol for some data points). For all time points, the % ID/g ratio of $\alpha_v\beta_6$-expressing tumor/control tumor remained >3:1. Activity in the negative control tumor was at the level of blood throughout.

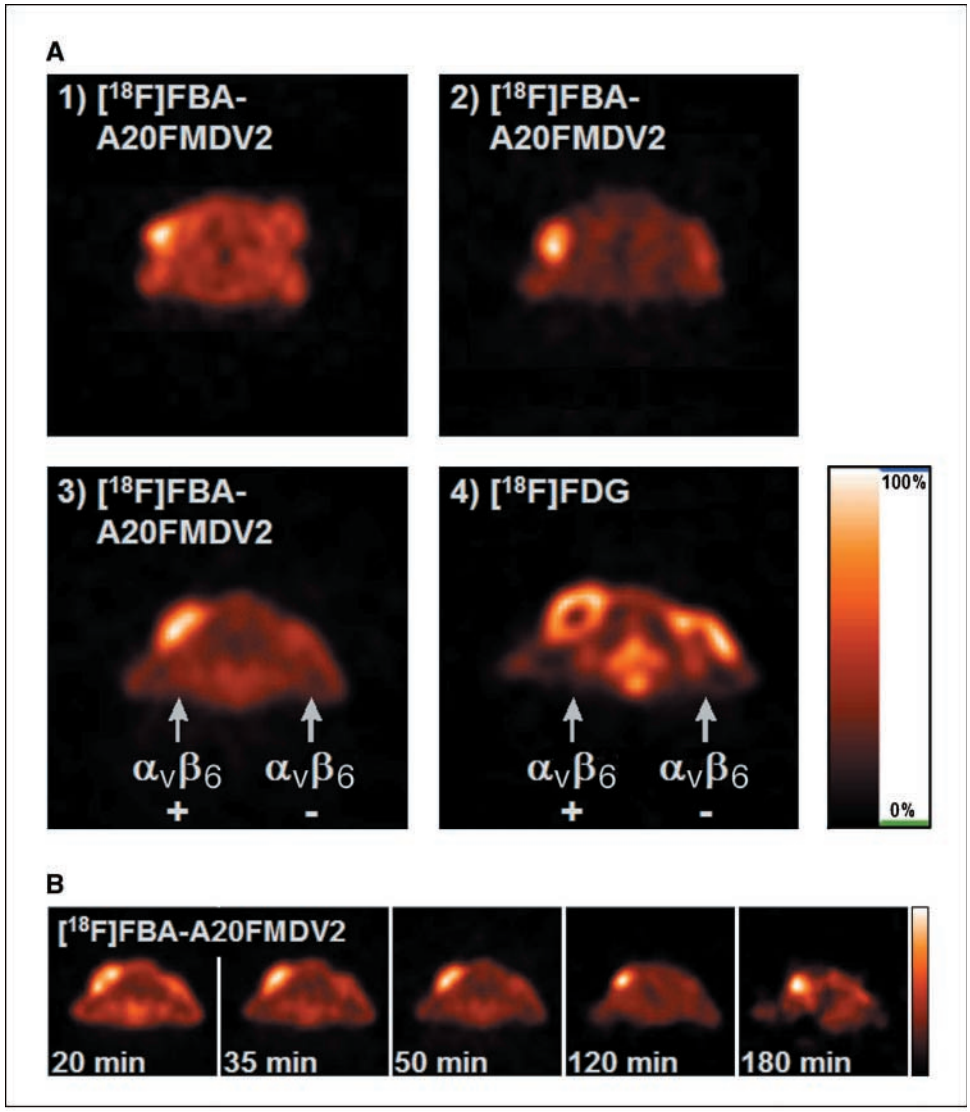

Figure 4. *A,* representative transaxial microPET images of [^{18}F]FBA-A20FMDV2 in three male *nu/nu* mice 45 min to 1 h after injection. The positive ($\alpha_v\beta_6$-expressing DX3puroβ6) tumors were located near the left shoulder, the negative (control DX3puro) tumors near the right shoulder. For comparison, *4* depicts a [^{18}F]FDG scan of the animal shown in *3*, obtained within 5 d. As expected, [^{18}F]FDG shows equal uptake in both tumors, in contrast to [^{18}F]FBA-A20FMDV2. *B,* transaxial microPET images obtained at various time points after injection of 143 μCi [^{18}F]FBA-A20FMDV2 in animal shown in (*A, 3*). The $\alpha_v\beta_6$-expressing tumor is clearly detectable as early as 20 min after injection. The later images reveal preferential retention of activity in the positive tumor. For each frame, the scale was set to range from 0% (no activity) to 100% (highest activity). The positive and negative tumors measured 6 $\times$ 11 mm and 7 $\times$ 8 mm maximum diameters, respectively.

different types of carcinoma compared with the corresponding normal tissue, $\alpha_v\beta_6$ represents a novel target for both imaging and therapy of cancer. We have developed and characterized a novel ^{18}F-labeled peptide tracer for the noninvasive imaging of $\alpha_v\beta_6$-positive cancers by PET. [^{18}F]FBA-A20FMDV2 selectively imaged $\alpha_v\beta_6$-positive tumors in mice bearing both $\alpha_v\beta_6$-positive and $\alpha_v\beta_6$-negative human xenografts. In cancers that express high levels of $\alpha_v\beta_6$ (e.g., OSCC), the use of noninvasive imaging to monitor tumor spread and recurrence will significantly improve the management of these diseases.

Acknowledgments

Received 3/19/2007; revised 6/5/2007; accepted 6/7/2007.

Grant support: DebRA grant (D. DiCara).

The costs of publication of this article were defrayed in part by the payment of page charges. This article must therefore be hereby marked *advertisement* in accordance with 18 U.S.C. Section 1734 solely to indicate this fact.

We thank D.L. Kukis for radionuclide production; C.E. Stanecki for help and advice with cell culture, flow cytometry, and ELISA; Dr. O.H. Aina for help with animal handling and data acquisition; Dr. C.A. Abbey and J.L. Choi for support with data analysis; Dr. A.D. Borowsky for help with tissue handling; Dr. K.S. Lam for use of the MALDI mass spectrometer; Dr. S. Simon for use of the flow cytometer; and the staff of the University of California Davis Center for Molecular and Genomic Imaging facility.

References

1. Cherry SR. The 2006 Henry N. Wagner lecture: of mice and men (and positrons)–advances in PET imaging technology. J Nucl Med 2006;47:1735–45.
2. Kelloff G, Hoffman JM, Johnson B, et al. Progress and promise of FDG-PET imaging for cancer patient management and oncologic drug development. Clin Cancer Res 2005;11:2785–808.
3. Kelloff GJ, Krohn KA, Larson SM, et al. The progress and promise of molecular imaging probes in oncologic drug development. Clin Cancer Res 2005;11:7967–85.
4. DiCara D, Rapisarda C, Sutcliffe JL, et al. Structure-function analysis of RGD-helix motifs in $\alpha_v\beta_6$ integrin ligands. J Biol Chem 2007;282:9657–65.
5. Hynes RO. Integrins: Bidirectional, allosteric signaling machines. Cell 2002;110:673–87.
6. Ruoslahti E. RGD and other recognition sequences for integrins. Annu Rev Cell Dev Biol 1996;12:697–715.
7. Haubner R. $\alpha_v\beta_3$-Integrin imaging: a new approach to characterise angiogenesis? Eur J Nucl Med Mol Imaging 2006;33:S54–63.
8. Meyer A, Auernheimer J, Modlinger A, Kessler H. Targeting RGD recognizing integrins: drug development, biomaterial research, tumor imaging, and targeting. Curr Pharm Des 2006;12:2723–47.
9. Haubner R, Wester HJ, Weber WA, et al. Noninvasive imaging of $\alpha_v\beta_3$ integrin expression using ^{18}F-labeled RGD-containing glycopeptide and positron emission tomography. Cancer Res 2001;61:1781–5.

10. Zhang XZ, Xiong ZM, Wu Y, et al. Quantitative PET imaging of tumor integrin $\alpha_v\beta_3$ expression with ^{18}F-FRGD2. J Nucl Med 2006;47:113–21.
11. Liu S. Radiolabeled multimeric cyclic RGD peptides as integrin $\alpha_v\beta_3$ targeted radiotracers for tumor imaging. Mol Pharmaceutics 2006;3:472–87.
12. Thomas GJ, Nystrom ML, Marshall JF. $\alpha_v\beta_6$ Integrin in wound healing and cancer of the oral cavity. J Oral Pathol Med 2006;35:1–10.
13. Breuss JM, Gallo J, Delisser HM, et al. Expression of the β_6 integrin subunit in development, neoplasia, and tissue-repair suggests a role in epithelial remodeling. J Cell Sci 1995;108:2241–51.
14. Kawashima A, Tsugawa S, Boku A, et al. Expression of α_v integrin family in gastric carcinomas: increased $\alpha_v\beta_6$ is associated with lymph node metastasis. Pathol Res Pract 2003;199:57–64.
15. Bates RC, Bellovin DI, Brown C, et al. Transcriptional activation of integrin β_6 during the epithelial-mesenchymal transition defines a novel prognostic indicator of aggressive colon carcinoma. J Clin Invest 2005;115:339–47.
16. Thomas GJ, Lewis MP, Hart IR, Marshall JF, Speight PM. $\alpha_v\beta_6$ integrin promotes invasion of squamous carcinoma cells through up-regulation of matrix metalloproteinase-9. Int J Cancer 2001;92:641–50.
17. Nystrom ML, McCulloch D, Weinreb PH, et al. Cyclooxygenase-2 inhibition suppresses $\alpha_v\beta_6$integrin-dependent oral squamous carcinoma invasion. Cancer Res 2006;66:10833–42.
18. Janes SM, Watt FM. New roles for integrins in squamous-cell carcinoma. Nat Rev Cancer 2006;6:175–83.
19. Rumboldt Z, Day TA, Michel M. Imaging of oral cavity cancer. Oral Oncol 2006;42:854–65.
20. Cancer Statistics Registrations: Series MB1 No. 21. Office of Population Censuses and Surveys (OPCS). London: HMSO; 1994.
21. Sutcliffe-Goulden JL, O'Doherty MJ, Marsden PK, Hart IR, Marshall JF, Bansal SS. Rapid solid phase synthesis and biodistribution of ^{18}F-labelled linear peptides. Eur J Nucl Med Mol Imaging 2002;29:754–9.
22. Marik J, Hausner SH, Fix LA, Gagnon MKJ, Sutcliffe JL. Solid-phase synthesis of 2-[^{18}F]fluoropropionyl peptides. Bioconjugate Chem 2006;17:1017–21.
23. Marik J, Sutcliffe JL. Click for PET: rapid preparation of [^{18}F]fluoropeptides using Cu^I catalyzed 1,3-dipolar cycloaddition. Tetrahedron Lett 2006;47:6681–4.
24. Marik J, Sutcliffe JL. Fully automated preparation of n.c.a. 4-[^{18}F]fluorobenzoic acid and *N*-succinimidyl 4-[^{18}F]fluorobenzoate using a Siemens/CTI chemistry process control unit (CPCU). Appl Radiat Isot 2007;65:199–203.
25. Guhlke S, Wester HJ, Bruns C, Stocklin G. (2-[^{18}F]fluoropropionyl-(D)phe(1))-octreotide, a potential radiopharmaceutical for quantitative somatostatin receptor imaging with PET—synthesis, radiolabeling, *in vitro* validation, and biodistribution in mice. Nucl Med Biol 1994;21:819–25.
26. Wüst F, Hultsch C, Bergmann R, Johannsen B, Henle T. Radiolabelling of isopeptide N^{ε}-(γ-glutamyl)-L-lysine by conjugation with *N*-succinimidyl-4-[^{18}F]fluorobenzoate. Appl Radiat Isot 2003;59:43–8.
27. Poethko T, Schottelius M, Thumshirn G, et al. Two-step methodology for high-yield routine radiohalogenation of peptides: ^{18}F-labeled RGD and octreotide analogs. J Nucl Med 2004;45:892–902.
28. Logan D, Abu-Ghazaleh R, Blakemore W, et al. Structure of a major immunogenic site on foot-and-mouth disease virus. Nature 1993;362:566–8.
29. Jackson T, Sheppard D, Denyer M, Blakemore W, King AMQ. The epithelial integrin $\alpha_v\beta_6$ is a receptor for foot-and-mouth disease virus. J Virol 2000;74:4949–56.
30. Monaghan P, Gold S, Simpson J, et al. The $\alpha_v\beta_6$ integrin receptor for foot-and-mouth disease virus is expressed constitutively on the epithelial cells targeted in cattle. J Gen Virol 2005;86:2769–80.
31. Burman A, Clark S, Abrescia NGA, Fry EE, Stuart DI, Jackson T. Specificity of the VP1 GH loop of foot-and-mouth disease virus for α_v integrins. J Virol 2006;80:9798–810.
32. Acharya R, Fry E, Stuart D, Fox G, Rowlands D, Brown F. The three-dimensional structure of foot-and-mouth disease virus at 2.9 Å resolution. Nature 1989;337:709–16.
33. Kraft S, Diefenbach B, Mehta R, Jonczyk A, Luckenbach GA, Goodman SL. Definition of an unexpected ligand recognition motif for $\alpha_v\beta_6$ integrin. J Biol Chem 1999;274:1979–85.
34. Mateu MG, Valero ML, Andreu D, Domingo E. Systematic replacement of amino acid residues within an Arg-Gly-Asp-containing loop of foot-and-mouth disease virus and effect on cell recognition. J Biol Chem 1996;271:12814–9.
35. Jackson T, King AMQ, Stuart DI, Fry E. Structure and receptor binding. Virus Res 2003;91:33–46.
36. Haubner R, Finsinger D, Kessler H. Stereoisomeric peptide libraries and peptidomimetics for designing selective inhibitors of the $\alpha_v\beta_3$ integrin for a new cancer therapy. Angew Chem Int Ed Engl 1997;36:1375–89.
37. Weinacker A, Chen A, Agrez M, et al. Role of the integrin $\alpha_v\beta_6$ in cell attachment to fibronectin—heterologous expression of intact and secreted forms of the receptor. J Biol Chem 1994;269:6940–8.
38. Hancock WS, Battersby JE. New micro-test for detection of incomplete coupling reactions in solid-phase peptide-synthesis using 2,4,6-trinitrobenzene-sulphonic acid. Anal Biochem 1976;71:260–4.
39. McCusker CF, Kocienski PJ, Boyle FT, Schatzlein AG. Solid-phase synthesis of c(RGDfK) derivatives: on-resin cyclisation and lysine functionalisation. Bioorg Med Chem Lett 2002;12:547–9.
40. Defrise M, Kinahan PE, Townsend DW, Michel C, Sibomana M, Newport DF. Exact and approximate rebinning algorithms for 3-D PET data. IEEE Trans Med Imag 1997;16:145–58.
41. Qi JY, Leahy RM, Cherry SR, Chatziioannou A, Farquhar TH. High-resolution 3D Bayesian image reconstruction using the microPET small-animal scanner. Phys Med Biol 1998;43:1001–13.
42. Marshall JF, Hart IR. The role of α_v-integrins in tumour progression and metastasis. Semin Cancer Biol 1996;7:129–38.
43. Gasteiger E, Hoogland C, Gattiker A, et al. Protein identification and analysis tools on the ExPASy server. In: Walker JM, editor. The proteomics protocols handbook. Totowa: Humana Press; 2005. Available from: http://www.expasy.org/tools/peptidecutter/.